European Journal of Neuroscience, Vol. 23, pp. 1839–1852, 2006 doi:10.1111/j.1460-9568.2006.04710.x

Enhanced perisomatic inhibition and impaired long-term potentiation in the CA1 region of juvenile CHL1-deficient mice

Alexander G. Nikonenko,[1,*] Mu Sun,[1,*,†] Eka Lepsveridze,[1] Ivayla Apostolova,[1] Iveta Petrova,[1] Andrey Irintchev,[1] Alexander Dityatev[1,2] and Melitta Schachner[1]
[1]Zentrum für Molekulare Neurobiologie, Universität Hamburg, Martinistrasse 52, D-20246 Hamburg, Germany
[2]Institut für Neurophysiologie und Pathophysiologie, Universitätsklinikum Eppendorf-Hamburg, Martinistrasse 52, D-20246 Hamburg, Germany

Keywords: electron microscopy, GABA, hippocampus, inhibitory synapses, parvalbumin interneurons, synaptic coverage

Abstract

The cell adhesion molecule, CHL1, like its close homologue L1, is important for normal brain development and function. In this study, we analysed the functional role of CHL1 in synaptic transmission in the CA1 region of the hippocampus using juvenile CHL1-deficient (CHL1–/–) and wild-type (CHL1+/+) mice. Inhibitory postsynaptic currents evoked in pyramidal cells by minimal stimulation of perisomatically projecting interneurons were increased in CHL1–/– mice compared with wild-type littermates. Also, long-term potentiation (LTP) at CA3–CA1 excitatory synapses was reduced under physiological conditions in CHL1-/– mice. This abnormality was abolished by application of a $GABA_A$ receptor antagonist, suggesting that enhanced inhibition is the cause of LTP impairment. Quantitative ultrastructural and immunohistochemical analyses revealed aberrations possibly related to the abnormally high inhibition observed in CHL1–/– mice. The length and linear density of active zones in symmetric synapses on pyramidal cell bodies, as well as number of perisomatic puncta containing inhibitory axonal markers were increased. Density and total number of parvalbumin-positive interneurons was also abnormally high. These observations and the finding that CA1 interneurons express CHL1 protein indicate that CHL1 is important for regulation of inhibitory synaptic transmission and interneuron populations in the postnatal brain. The observed enhancement of inhibitory transmission in CHL1–/– mice is in contrast to the previous finding of reduced inhibition in L1 deficient mice and indicates different functions of these two closely related molecules.

Introduction

The cell recognition molecule, CHL1, close homologue of L1, is expressed in the nervous system and, as shown in mice, its expression is developmentally regulated (Holm *et al*., 1996; Hillenbrand *et al*., 1999). CHL1 expression is detectable early during embryonic development (day 13), reaches peak levels around birth and declines to lower levels in the adult mouse brain. CHL1 is not only widely expressed in neurons, similar to L1, but also in astrocytes and oligodendrocyte precursor cells. After injury of the central and peripheral nervous system, expression of CHL1 is up-regulated in neuronal and glial cells (Chaisuksunt *et al*., 2000a, b; Zhang *et al*., 2000; Rolf *et al*., 2003). *In vitro*, CHL1 promotes neurite outgrowth of hippocampal and cerebellar neurons (Hillenbrand *et al*., 1999).

Studies on CHL1-deficient (CHL1–/–) mice have shown the importance of this glycoprotein for neurodevelopment (Montag-Sallaz *et al*., 2002). CHL1 deficiency causes alterations in the hippocampal mossy fibre and olfactory axon projections. Behavioural analyses have indicated that CHL1–/– mice react differently to novel stimuli. CHL1 is also important for cortical development (Demyanenko *et al*., 2004). In CHL1-deficient mice, the pyramidal neurons in layer V of the visual cortex are deeply displaced and have inverted polarity, while neurons in the somatosensory cortex have improperly orientated apical dendrites.

The *CHL1* gene in humans maps to chromosome region 3p26.1, which has been associated with intelligence and cognition. Identification of a patient with nonspecific mental retardation and a mutation in the *CHL1* gene has provided direct evidence for the linkage of the *CHL1* locus to mental functions (Frints *et al*., 2003). Linkage analyses have suggested that CHL1 may be one of the susceptibility factors for schizophrenia (Sakurai *et al*., 2002; Lewis *et al*., 2003; Chen *et al*., 2005). Similar to schizophrenia patients, CHL1–/– mice are impaired in prepulse inhibition (Irintchev *et al*., 2004), a measure for the ability of the central nervous system to gate the flow of sensory information (Van den Buuse *et al*., 2003).

L1 has been, like CHL1, linked to mental retardation (Kenwrick *et al*., 2000) and schizophrenia (Kurumaji *et al*., 2001) and prepulse inhibition in L1-deficient mice is reduced (Irintchev *et al*., 2004). Deficiencies in both genes lead to malformations of the hippocampus (Demyanenko *et al*., 1999; Montag-Sallaz *et al*., 2002). In a previous study we found that perisomatic inhibitory synaptic transmission is reduced in the CA1 region of L1 null mice (Saghatelyan *et al*., 2004).

Correspondence: Dr Melitta Schachner, as above.
E-mail: melitta.schachner@zmnh.uni-hamburg.de

*A.G.N and M.S. contributed equally to this work.

†*Present address*: Howard Hughes Medical Institute, University of Minnesota, USA.

Received 26 April 2005, revised 25 January 2006, accepted 30 January 2006

This abnormality is noteworthy in light of consistent findings of reduced numbers of GABAergic cells and lower expression levels of inhibitory cell markers in major psychiatric diseases (Lewis *et al.*, 2005; Torrey *et al.*, 2005). Because of the high homology of CHL1 to L1 and expression of CHL1 in hippocampal interneurons (Hillenbrand *et al.*, 1999), we investigated the role of CHL1 in inhibitory synaptic transmission in the hippocampus. The physiological and morphological data obtained in this study indicate that synaptic inhibition is abnormally enhanced in the CA1 region of CHL1-deficient mice.

Materials and methods

Animals

For analysis of electrophysiological parameters, age-matched 2–4-week-old CHL1–/– mice on a C57BL/6J genetic background of both sexes were used (Montag-Sallaz *et al.*, 2002). For immunohistochemistry and electron microscopic analysis, 4- and 3-week-old mice were used, respectively. Sex- and age-matched wild-type littermates (CHL1+/+) served as controls. All experiments were conducted in accordance with the German and European Community laws on protection of experimental animals and the procedures used were approved by the local authorities of the City of Hamburg.

Slice preparation for electrophysiological recordings

Transverse slices of the hippocampus (350-μm thick) were used for patch-clamp and field excitatory postsynaptic potential (fEPSP) recordings. After halothane anaesthesia and decapitation of the animals, the brains were dissected and cut on a Leica VT 1000M vibratome (Leica, Nussloch, Germany) in ice-cold artificial cerebrospinal fluid (ACSF) containing (in mM): 250 sucrose, 25 $NaHCO_3$, 25 glucose, 2.5 KCl, 1.25 NaH_2PO_4, 2 $CaCl_2$, 1 $MgCl_2$ (pH 7.3, adjusted with NaOH). The slices were kept at room temperature in Carbogen (95% O_2, 5% CO_2)-aerated ACSF, containing 125 mM NaCl instead of 250 mM sucrose, for at least two hours before the start of recordings.

Patch-clamp recordings in hippocampal slices

Submerged slices were continuously superfused in a recording chamber with Carbogen-aerated ACSF (2–3 mL/min) at room temperature. All measurements were performed blindly with respect to genotypes. Cells in the CA1 region were visualized using infrared microscopy (BX50WI, Olympus Optical Co., Hamburg, Germany) and the patch-clamp technique was used for whole-cell recordings of synaptic currents from pyramidal cells at a holding potential of −60 mV (Saghatelyan *et al.*, 2001, 2004). To record inhibitory postsynaptic currents (IPSCs), the intracellular Cl^- concentration was elevated (60 mM KCl, 85 mM K-gluconate), thus increasing the driving force of $GABA_A$ receptor-mediated Cl^- currents. To evoke perisomatic IPSCs, the stimulating glass electrode with a resistance of 2 MΩ was placed in the stratum pyramidale and 0.2-ms-long pulses were delivered using a stimulus isolator (WPI, Sarasota, USA). Miniature and evoked IPSCs were isolated by application of antagonists of AMPA and NMDA receptors, CNQX (25 μM) and AP-5 (50 μM, Tocris, Bristol, UK), respectively. The Na^+-channel blocker TTX (1 μM, Roth, Karlsruhe, Germany) was additionally included in the extracellular solution to record miniature IPSCs. These were detected using the template method implemented in the AxoGraph 4.0 software (Axon Instruments, Foster City, CA, USA), as events with signal-to-noise ratio greater than three. Whole-cell voltage clamp recordings were performed using an EPC-9 amplifier (Heka Electronik, Lambrecht/Pfalz, Germany) and patch clamp pipettes with a resistance of 2.5–3.5 MΩ. Serial resistance in whole-cell configuration was approximately 15 MΩ.

Analysis of unitary and composite pIPSCs

Putative unitary perisomatic inhibitory postsynaptic currents (pIPSCs) were recorded in response to minimal stimulation, as previously described (Stevens & Wang, 1994; Saghatelyan *et al.*, 2001, 2004). To set the minimal stimulus intensity, presumably activating a single presynaptic neuron, the stimulus–response curves were determined and only pIPSCs within a clearly defined first plateau were selected for the analysis. To investigate use-dependent modulation of synaptic efficacy, paired-pulse stimulation or ten stimuli with intervals of 10, 20, 50, 100 and 200 ms were applied 10–20 times. The trains were followed by a single pulse applied 200 ms after the last stimulus to monitor recovery of IPSCs. To avoid effects of presynaptic $GABA_B$ receptors, the $GABA_B$ receptor antagonist CGP54626 (200 nM; Biotrend, Cologne, Germany) was bath applied during these experiments. The amplitudes of IPSCs were measured using an average of 10–30 sweeps.

Recordings of LTP

Field EPSPs (fEPSPs) were recorded by glass pipettes filled with ASCF and having a resistance of 2–3 MΩ. Stimulation was applied by unipolar stimulating glass electrodes with a broken tip and resistance less then 1 MΩ. Basal synaptic transmission was monitored at 0.033 Hz. Responses were amplified and filtered at 1 kHz using CyberAmp 320 (Axon Instruments). Data acquisition and analysis was performed using the Pulse program (Heka Electronik). Amplitude of responses was measured as a function of stimulation intensity that was stepwise increased by 10 or 20 μA until population spike was elicited. Paired-pulse facilitation (PPF) was defined as A2/A1 × 100, where A1 and A2 are the amplitudes of the fEPSPs evoked by the first and second pulse, respectively. Long-term potentiation (LTP) was induced by five theta-burst stimulations delivered every 20 s. Each theta-burst stimulation consisted of ten bursts delivered at 5 Hz. Each burst was composed of four stimuli delivered at 100 Hz; the duration of pulses was 0.2 ms. Amplitudes of three consecutive fEPSPs were averaged and these mean values were used to compute profiles of LTP. The mean amplitude of fEPSPs recorded 0–10 min before TBS was set to 100%. The values of short-term potentiation were calculated as maximal potentiation during the first minute after LTP induction. LTP levels were calculated as the increase in the mean amplitudes of fEPSPs measured 50–60 min after induction of LTP.

Tissue processing for electron microscopic analysis

Five CHL1–/– and five CHL1+/+ mice were anaesthetized with Narcoren® (Merial, Hallbermoos, Germany, 5 μL/g body weight, i.p.) and perfused transcardially with a mixture of 4% formaldehyde and 2.5% glutaraldehyde in 0.1 M phosphate buffer (pH 7.4). After perfusion, the brains were dissected and postfixed overnight at 4 °C in 4% formaldehyde and 5% glutaraldehyde in the same buffer. On the next day, the specimens were embedded in agar and 100-μm-thick transverse slices were cut on a vibratome. The sections were postfixed for 1.5 h in 1% OsO_4 in 0.1 M cacodylate buffer, dehydrated and flat embedded in Epon. Before sectioning, the slices were fixed onto Epon

blocks by instant cyanocrylate glue Roti®-Coll1 (Carl Roth, Karlsruhe, Germany).

Coverage of pyramidal cell bodies by active zones of symmetric synapses

An estimate of surface ratio was used to stereologically quantify the length of apposition between CA1 pyramidal cell bodies and active zones of symmetric synapses in tissue sections. Semi-thin sections were used to locate the CA1 pyramidal cell layer. The slice was then detached from the Epon block, given a random rotation in the horizontal plane and re-glued onto the Epon block to ensure sectioning perpendicular to the horizontal plane of the slice. Semi-thin sections were cut once again to check the location of the pyramidal cell layer. A pyramid was then trimmed, and 70-nm-thick ultrathin random sections were prepared with a diamond knife. Sections were collected on 300 mesh copper grids, counterstained with uranyl acetate and lead citrate and observed on a Zeiss EM902A transmission electron microscope (Zeiss, Oberkochen, Germany).

At least ten electron micrographs of the CA1 pyramidal cell layer were taken per mouse at a magnification of ×7000. The negatives were digitized using a flatbed scanner at 600 dots per inch (dpi) and 256 grey levels, and digitally inverted. The surface ratio was calculated according to Howard & Reed (1998) as the ratio of the surface densities of the active zone and perisomatic plasma membrane profiles and expressed as a percentage. Active zones of symmetric synapses (Gray's type one) were identified by the presence of a postsynaptic density that was equal to the density of the presynaptic side (Peters *et al*., 1991). Ten images of the CA1 pyramidal cell layer per animal were sampled with a test grid. Linear density of perisomatic active zones was estimated as the number of active zone profiles per unit length of the pyramidal cell body profile. Fifteen measurements were made per animal and thus 75 measurements per animal group.

Size of active zones and number and spatial arrangement of synaptic vesicle profiles in perisomatic symmetric synapses

The length of the synaptic density profile was used as a measure of the active zone size of perisomatic synapses in the CA1 pyramidal cell layer. Measurements were performed using the UTHSCSA ImageTool program 2.0 (University of Texas, San Antonio, TX, USA; ftp://maxrad6.uthscsa.edu), and digital electron micrographs of the CA1 pyramidal cell layer were taken at a magnification of ×30 000 and captured with a MegaView II (Soft Imaging System GmbH, Munster, Germany) digital camera attached to the Zeiss EM902A microscope. At least ten synaptic profiles were analysed per mouse. The *x*-, *y*-coordinates of vesicle profile centres were registered using digital images and the UTHSCSA ImageTool program. Coordinate samples were analysed with the first nearest neighbour distance (NND) algorithm using original software written in Delphi (version 5, Borland Software Corp., Scotts Valley, CA, USA) by Alexander G. Nikonenko. In our sampling scheme, spatial arrangement of synaptic vesicles was analysed in ten presynaptic boutons per animal (50 terminals per animal group). In addition, the measurements of the distance between the centre of a vesicle profile and the nearest point tracing the active zone profile were performed using the original LoClust software written in Delphi by Alexander G. Nikonenko. Synaptic vesicle numbers were counted for the whole presynaptic terminal and per vesicle pool located within 100 nm of the active zone of a synapse. Measurements were performed in ten presynaptic terminals per animal (50 terminals per animal group). All ultrastructural analyses were performed in a blind fashion.

Immunohistochemistry and in situ *hybridization*

Tissue preparation and immunohistochemical stainings were performed as described previously (Irintchev *et al*., 2005). Four-week-old mice were anaesthetized with Narcoren® and transcardially perfused with physiologic saline for 60 s followed by fixative [4% formaldehyde and 0.1% $CaCl_2$ in 0.1 M cacodylate buffer, pH 7.3, 15 min at room temperature (RT)]. Brains were postfixed overnight (18–22 h) at 4 °C in the fixative solution supplemented with 15% sucrose, followed by immersion in 15% sucrose solution in 0.1 M cacodylate buffer, pH 7.3, for an additional day at 4 °C. The tissue was frozen for 2 min in 2-methyl-butane (isopentane) precooled to −30 °C in the cryostat. Serial coronal sections of 25-μm thickness were obtained from the whole brain on a cryostat (Leica CM3050). Sections were collected on SuperFrost®Plus glass slides (Roth, Karlsruhe, Germany) so that four sections 250 μm apart were present on each slide.

The following commercially available antibodies were used at optimal dilutions: anti-mouse CHL1 (goat polyclonal antibody, R & D Systems, Wiesbaden, Germany, 1 : 200), anti-parvalbumin (mouse monoclonal antibody, clone PARV-19, Sigma, Taufkirchen, Germany, 1 : 1000) and anti-vesicular GABA transporter (VGAT, rabbit polyclonal antibody, Synaptic Systems, Göttingen, Germany, 1 : 1000). Prior to the staining, antigen de-masking using 0.01 M sodium citrate solution (pH 9.0) was carried out in a water bath (80 °C, 30 min; Jiao *et al*., 1999). Blocking of nonspecific binding sites was performed for 1 h at RT using phosphate-buffered saline (PBS, pH 7.3) containing 0.2% Triton X-100, 0.02% sodium azide and 5% normal serum from the species in which the secondary antibody was produced. Incubation with the primary antibody, diluted in PBS containing 0.5% lambda-carrageenan and 0.02% sodium azide, was carried out at 4 °C for 3 days. After washing in PBS (3 × 15 min at RT), the appropriate secondary antibody conjugated with Cy3 (Jackson ImmunoResearch Laboratories, Dianova, Hamburg, Germany) diluted 1 : 200 in PBS-carrageenan solution was applied for 2 h at RT. Finally, the sections were washed, incubated for 10 min at RT with bis-benzimide solution (Hoechst 33258 dye, 5 μg/mL in PBS, Sigma) to stain cell nuclei and mounted under coverslips with anti-fading medium (Fluoromount G, Southern Biotechnology Associates, Biozol, Eching, Germany).

To visualize perineuronal nets, *Wisteria floribunda* agglutinin (WFA) staining was performed according to the immunohistochemical protocol described above using biotin-conjugated WFA (Sigma, 1 : 500) and Cy2-streptavidin (1 : 200 in PBS, Jackson ImmunoResearch). For double labelling, biotinylated WFA and antibody against CHL1 or parvalbumin (PV) were mixed at optimal dilutions. Visualization was made with streptavidin-Alexa Fluor® 488 (Molecular Probes, Leiden, The Netherlands) and anti-goat or anti-mouse IgG–Cy3. Double immunostaining for PV and VGAT was performed by mixing the primary antibodies at optimal dilutions and using a Cy3-conjugated anti-mouse and a Cy2-labelled anti-rabbit secondary antibody preabsorbed with rabbit and mouse serum proteins, respectively (multiple-labelling grade antibodies, Jackson ImmunoResearch). For a given antigen, all sections were stained in the same solution kept in screw-capped staining plastic jars (capacity 35 mL, ten slides, Roth). Specificity of staining was tested by omitting the first antibody or replacing it by variable concentrations of normal serum or IgG. For the CHL1 antibody, specificity was also controlled by staining tissue sections from CHL1 deficient mice (Fig. 6B; see also Supplementary material Fig. S1, A and B).

Digoxigenin-labelled antisense cRNA probe corresponding to the extracellular domain of CHL1 was prepared as described previously (Holm *et al.*, 1996). A sense probe was transcribed from a similar construct with inserts in the opposite direction. The cRNA probes were generated using T7 RNA polymerase followed by alkaline treatment to obtain an average fragment length of 250 nucleotides. *In situ* hybridization was performed as described (Bartsch *et al.*, 1992; Dörries *et al.*, 1993) using 70-μm-thick vibratome sections from formaldehyde-fixed (see above) brains of wild-type mice of different ages (1 week to 1 year, $n = 14$).

Light-microscopic analysis of perisomatic puncta and pyramidal cell size

Estimation of perisomatic puncta and area of pyramidal cell bodies was performed as previously described (Irintchev *et al.*, 2005). Stacks of images of 1-μm thickness were obtained from sections double-stained for PV and VGAT on a LSM 510 confocal microscope (Zeiss) using 63× oil immersion objective and 1024 × 1024 pixel digital resolution. One merged image (red and green channel) per cell at the level of the largest cell body cross-sectional area was used to measure soma perimeter and area and to count individually discernible perisomatic puncta (Fig. 6A). Numbers of PV^+ $VGAT^+$ and PV^- $VGAT^+$ puncta (see Results for further details) were normalized to the perimeter of the cell profile. These measurements were performed using the ImageTool software.

Quantitative analysis of parvalbumin-positive interneurons and pyramidal neurons

Numerical densities were estimated using the optical disector method (Gundersen, 1986) as previously described (Irintchev *et al.*, 2005). Counting was performed on an Axioskop microscope (Zeiss) equipped with a motorized stage and Neurolucida software-controlled computer system (MicroBrightField Europe, Magdeburg, Germany). Serial sections spaced 250 μm apart from the dorsal hippocampus were used for the quantifications. Bregma −2.18 mm was defined as the border between the dorsal and ventral hippocampus, a point after which, in the rostro-caudal direction, the CA3 region rapidly gains a tangential orientation with respect to the plane of sectioning (Franklin & Paxinos, 1997). The volume of the whole CA1 region and of its pyramidal layer was estimated using the Cavalieri method. The borders of the CA1 region were defined by the nuclear staining pattern (Plan-Neofluar® 10×/0.3 objective) according to criteria described by Long *et al.* (1998). The numerical density of parvalbumin-positive (PV^+) cells was estimated by counting nuclei of immunolabelled cells within systematically randomly spaced optical disectors throughout the whole CA1 area. The parameters for this analysis were: guard space depth 2 μm, base and height of the disector 3600 μm^2 and 10 μm, respectively, distance between the optical disectors 60 μm, objective 40× Plan-Neofluar® 40×/0.75. The same parameters were used for the counting of nuclei in the pyramidal layer except for the base of the disector, which was 625 μm^2 and the space between disectors (25 μm). Nuclei of glial cells in the pyramidal layer were easily recognized and were not counted. Left and right hippocampal areas were evaluated in four sections each. All results shown are averaged bilateral values. The counts were performed on coded preparations by one observer.

Statistical analysis

All numerical data are presented as group mean values with standard errors of the mean (SEM). Group mean values were calculated from individual mean values so that the degrees of freedom were determined by the number of sampling units (animal, tissue, slice). Parametric tests (*t*-test, one- and two-way analysis of variance, ANOVA) were used to compare group mean values. The data used for such analyses conformed to the requirement for normal distribution ('normality' test, SigmaStat 2.0, SPSS, Chicago, IL, USA). Distributions were analysed with the nonparametric two-tailed Kolmogorov–Smirnov test. The threshold value for acceptance of differences was 5%.

Results

Basal synaptic transmission and use-dependent modulation of perisomatic inhibitory currents

Perisomatic inhibitory transmission was studied by recording of putative unitary pIPSCs in response to minimal stimulation of interneurons. The recordings were performed in the presence of antagonists of glutamate receptors, CNQX and AP-5, in order to block EPSCs. For analysis, only pIPSCs within a defined first-level plateau of responses to stimuli of varying intensities were selected (Fig. 1A) (Stevens & Wang, 1994; Saghatelyan *et al.*, 2001, 2004). The pIPSCs had short and stable latencies, which were similar for both genotypes (1.9 ± 0.18 ms and 2.0 ± 0.13 ms for CHL1+/+ and CHL1–/– mice, respectively, $n = 12$ per genotype, $P > 0.05$, two-sided *t*-test for independent samples). The analysed pIPSCs lacked visible deflections during the rising phase, as one would expect for unitary currents evoked by stimulation of a single interneuron. The pIPSCs in both genotypes had similar shapes (Fig. 1B) with a half-width of 45 ± 2.8 ms vs. 50 ± 3.5 ms and a short rise-time of 1.8 ± 0.19 ms vs. 1.8 ± 0.09 ms in CHL1+/+ and CHL1–/– mice, respectively ($P > 0.05$, *t*-tests). Such short rise-times are characteristic of perisomatic inhibitory currents and allows them to be distinguished from dendritic currents (Banks *et al.*, 1998; Saghatelyan *et al.*, 2000). In contrast to the similarity in latency and shape, the mean amplitude of pIPSCs was largely increased (+53%) in CHL1-deficient mice compared with wild-type littermates (Fig. 1C; 138 ± 18 pA vs. 90 ± 10 pA; $P < 0.01$, *t*-test). The stimulation currents required to elicit the pIPSCs were similar for both genotypes (Fig. 1C).

As increase in pIPSCs can result from larger quantal size of postsynaptic responses produced by a single vesicle release, we analysed amplitudes of miniature IPSCs (mIPSCs), which provide a direct measure of the quantal size (Fig. 2A). The frequency distributions of mIPSC amplitudes were similar in CHL1+/+ and CHL1–/– mice (Fig. 2B; $P > 0.05$, Kolmogorov–Smirnov test). No difference between the genotypes was also found for mean amplitudes of the mIPSCs (Fig. 2C; $P > 0.05$, *t*-test). Normal quantal size and increased mean amplitude of unitary pIPSCs in CHL1–/– mice indicate that the quantal content, i.e. number of quanta released in response to an action potential invading the perisomatic terminal, is increased in the mutant animals. In contrast to the increased evoked IPSCs, the frequency of the mIPSCs, reflecting the spontaneous release probability, in CHL1–/– mice was similar to that in CHL1+/+ littermates (Fig. 2D; $P > 0.05$, *t*-test).

To analyse use-dependent modulation of perisomatic inhibitory transmission, we recorded pIPSCs in response to paired-pulse and short tetanic stimulations (Fig. 3A and C). The interstimulus interval (ISI) varied between 10 ms and 200 ms. Paired-pulse stimulation with 10 and 20 ms intervals produced a depression down to 30–60% in both genotypes (Fig. 3B). The depression was even stronger (to 20%) during tetanic stimulation with these intervals (Fig. 3D), presumably

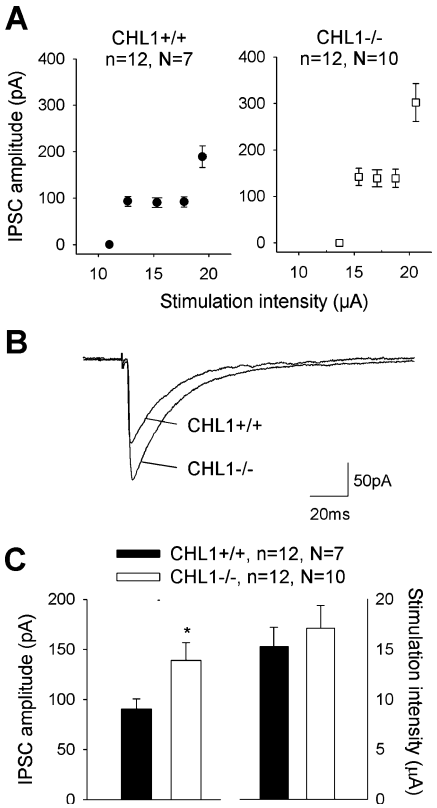

FIG. 1. Analysis of minimal pIPSCs. (A) Stimulus–response plots for CHL1+/+ and CHL1–/– mice. (B) Minimal pIPSCs obtained by averaging of 30 consecutive sweeps recorded in single pyramidal neurons in CHL1+/+ and CHL1–/– mice. IPSCs were evoked by an electrode placed close to the recorded cell in the stratum pyramidale of CA1 and were isolated by perfusion of slices with 25 μM CNQX and 50 μM AP-5. (C) Mean amplitudes of unitary pIPSCs and stimulation intensity (+ SEM) used to elicit these IPSCs in CHL1+/+ and CHL1–/– mice. *$P < 0.05$, *t*-test, comparing group mean values. Numbers of analysed cells (*n*) and animals (*N*) are indicated.

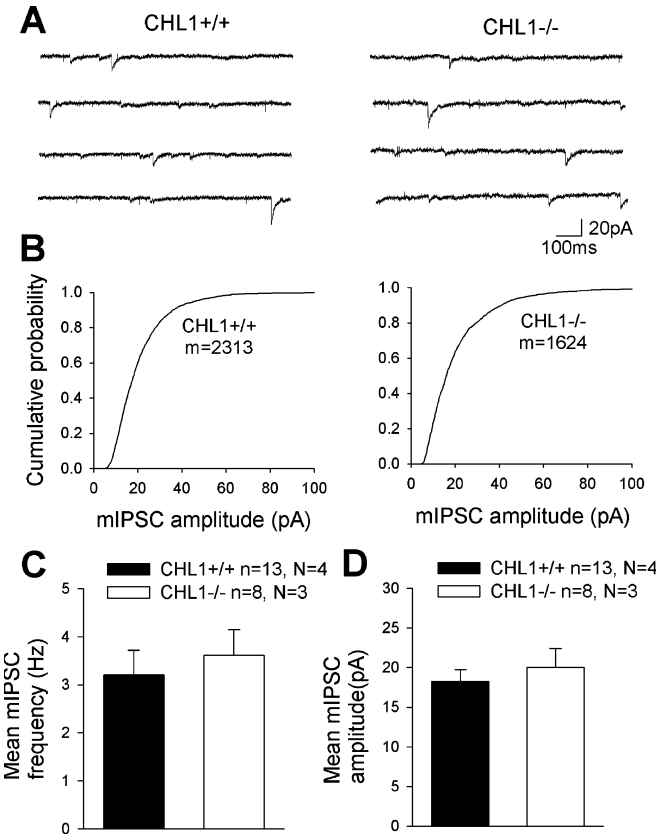

FIG. 2. Analysis of mIPSCs. (A) Examples of mIPSCs isolated in CHL1–/– and CHL1+/+ mice by perfusion with 1 μM TTX, 25 μM CNQX and 50 μM AP-5. (B) Cumulative distributions of mIPSC amplitude in CHL1–/– and CHL1+/+ mice. The number of measured amplitudes is indicated by *m*. No difference between the two distributions was detected by the Kolmogorov–Smirnov test ($P > 0.05$). (C and D) Mean amplitudes (C) and frequencies (D) + SEM of mIPSCs recorded in cells from CHL1–/– and CHL1+/+ mice. Numbers of analysed cells (*n*) and animals (*N*) are indicated.

due to higher depletion of vesicles after ten pulses as compared with two pulses. At 50, 100, and 200 ms ISIs, paired-pulse depression was only to approximately 80% of the baseline level and tetanic depression was down to 50% in both genotypes (Fig. 3A–D). IPSCs recorded 200 ms after the tetanus showed recovery to approximately 50–60% level at all ISIs and in both genotypes (Fig. 3E). The recorded profiles of depression in CHL1–/– mice very much resembled those previously reported for wild-type mice (Saghatelyan *et al.*, 2004). In CHL1+/+ mice, two cells showed paired-pulse facilitation at short ISIs, unlike other cells. Therefore, the mean values of paired-pulse modulation at 10 and 20 ms had a tendency to be higher in CHL1+/+ than in CHL1+/+ mice. Independently of whether these two cells were taken for the statistical evaluation or not, two-way variance analysis (ANOVA for independent factor genotype and repeated measure ISI) of paired-pulse modulation in CHL1–/– and CHL1+/+ mice revealed no significant effects of genotype and no interaction between genotype and ISI ($P > 0.1$; Fig. 3B). Also for tetanic and post-tetanic depression, there was no detectable effects of genotype and no interaction between genotype and ISI ($P > 0.1$; Fig. 3D and E). Application of the *t*-test with Bonferroni correction for multiple comparisons also did not reveal any significant difference between genotypes for any tested ISI. In summary, no significant abnormalities in activity-dependent modulation was found in CHL1–/– mice.

LTP in CA3–CA1 synapses

As GABAergic transmission appeared to be increased in CHL1–/– mice, we hypothesized that this abnormality may result in a reduction of LTP. To verify this hypothesis, we stimulated axons of CA3 neurons and recorded field excitatory postsynaptic potentials (fEPSPs) in the stratum radiatum of the CA1 region. As shown in Fig. 4A, no difference was found in stimulus–response curves, i.e. in the relationships between amplitude of fEPSPs and intensity of stimulation, between CHL1+/+ and CHL1–/– mice. Comparison of paired-pulse facilitation with 10, 20, 50, 100 and 200 ms ISIs using two-way ANOVA also did not reveal abnormalities in CHL1–/– mice compared with CHL1+/+ littermates (Fig. 4B). However, short-term potentiation and LTP evoked by five trains of theta-burst stimulation (TBS) were significantly reduced in CHL1–/– as compared with CHL1+/+ mice (144 ± 4.2% vs. 178 ± 9.1% and 124 ± 3.1% vs. 148 ± 4.5% in CHL1–/– and CHL1+/+ mice, respectively, $P < 0.01$, *t*-test; Fig. 4C). To verify whether the LTP deficit in CHL1–/– mice was due to increased GABAergic inhibition, we studied LTP after blocking of the $GABA_A$ receptors with picrotoxin. Short-term potentiation and LTP recorded in the presence of picrotoxin were similar in CHL1–/– mice and CHL1+/+ littermates (203 ± 17% vs. 171 ± 8.4% and 152 ± 3.1% vs. 162 ± 11% in CHL1–/– and CHL1+/+ mice, respectively, $P > 0.05$, *t*-test). Therefore, the LTP deficit in CA3–CA1 synapses of CHL1-deficient mice can be attributed to enhanced GABAergic transmission.

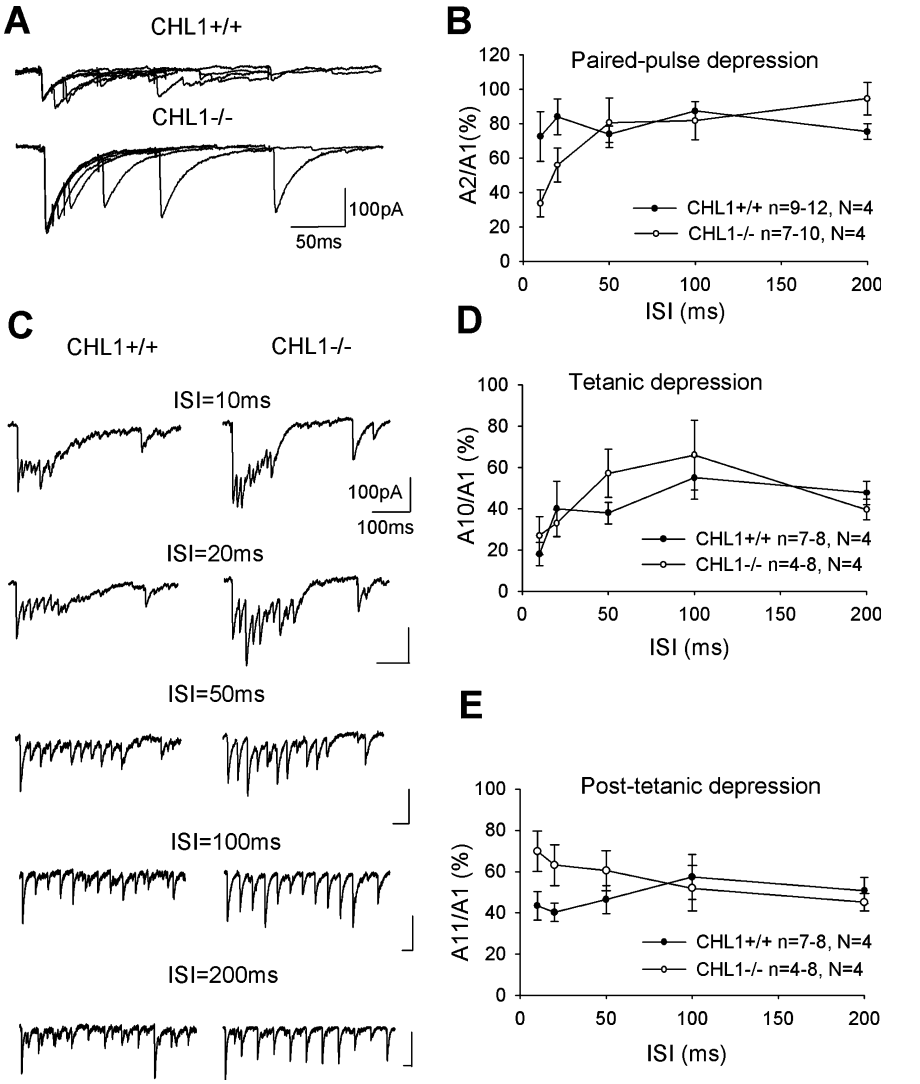

FIG. 3. Use-dependent modulation of pIPSCs. (A) Superposition of composite pIPSCs evoked by paired-pulse stimulation with intervals of 10, 20, 50, 100 and 200 ms in CHL1+/+ and CHL1–/– mice. (B) Mean values ± SEM of paired-pulse depression of composite pIPSCs in CHL1+/+ and CHL1–/– mice. Depression was calculated as the ratio of the second to the first pIPSC amplitude (A2/A1) as a percentage. (C) Depression of composite pIPSCs evoked by short tetanic stimulations (ten pulses with interstimulus intervals, ISI, of 10, 20, 50 and 100 ms), followed by a single pulse after 200 ms. Scale bars indicate 100 pA and 100 ms and are valid for both the CHL1–/– and CHL1+/+ traces shown. (D and E) Mean values ± SEM of tetanic (D) and post-tetanic (E) depression of composite pIPSCs in CHL1+/+ and CHL1–/– mice. The ratio between amplitudes of IPSPs evoked by the last (10th) stimulus and the first stimulus in the train (A10/A1) was used as a measure of tetanic depression (D). The ratio between amplitudes of pIPSCs evoked by the 11th pulse 200 ms after the train and the first stimulus in the train (A11/A1) was used as a measure of post-tetanic depression (E). Numbers of analysed cells (*n*) and animals (*N*) are indicated.

Ultrastructural analysis of perisomatic synapses

Qualitatively, no differences were noticed in the fine structure of symmetric, putative inhibitory, perisomatic synapses on principal neurons in the CA1 region of CHL1-deficient mice and wild-type littermates. Figure 5A shows an example of a symmetric synapse in a CHL1–/– mouse in which no apparent abnormalities can be detected. Quantitative analyses revealed, however, large differences between the genotypes in the synaptic coverage of the pyramidal cell bodies. The frequency of synaptic contacts on the surface of the perikarya, as estimated by linear density of active zones (number per unit cell membrane length) and surface ratio of active zones (percentage of cell body surface covered by active zones), was by 46% and 52% higher, respectively, in the mutant mice compared with wild-type animals (Fig. 5B, 'Density' and 'Surface ratio'). Also, the average length of the active zones was increased in CHL1–/– mice (+19% compared with CHL1+/+ animals, Fig. 5B, 'Length').

We also estimated a number of parameters at the level of individual synapses. The average area of the presynaptic terminal profiles and number of synaptic vesicles per terminal profile did not differ in the two animal groups (0.70 ± 0.18 μm^2 vs. 0.80 ± 0.06 μm^2 and 53 ± 10 vs. 68 ± 13 in CHL1+/+ and CHL1–/– mice, respectively, $P > 0.05$, *t*-tests). Accordingly, no difference was found in the density (number per unit area) of synaptic vesicles (Fig. 5C, 'Density'). On the average, the shortest distance of a synaptic vesicle to an active zone (Fig. 5C, 'Distance to AZ') or to the first nearest neighbour (56 ± 0.84 vs. 56 ± 0.74 nm in CHL1+/+ and CHL1–/– mice, respectively, $P > 0.05$, *t*-test) were also similar in the two genotype groups. Despite similar mean values for the nearest neighbour distances in the two groups, the variance of these distances was smaller in the CHL1–/– mice (−28% compared with CHL1+/+ littermates, Fig. 5C, 'NN variance'). This indicates increased homogeneity in spacing between individual synaptic vesicles in CHL1–/– synapses and, thus, altered spatial arrangement. Altered spatial distribution of synaptic vesicles in mutant mice was also indicated by the observation of higher numbers of vesicles per terminal close to (at distances smaller than 100 nm) active zones in CHL1–/– mice compared with CHL1+/+ littermates (+27%, Fig. 5C, 'Vesicles < 100 nm').

Light-microscopic immunohistochemical analysis of perisomatic puncta

The electron-microscopic data indicated that the inhibitory synaptic input to the cell bodies of CA1 principal cells was significantly increased in CHL1-deficient mice. This input is provided by two

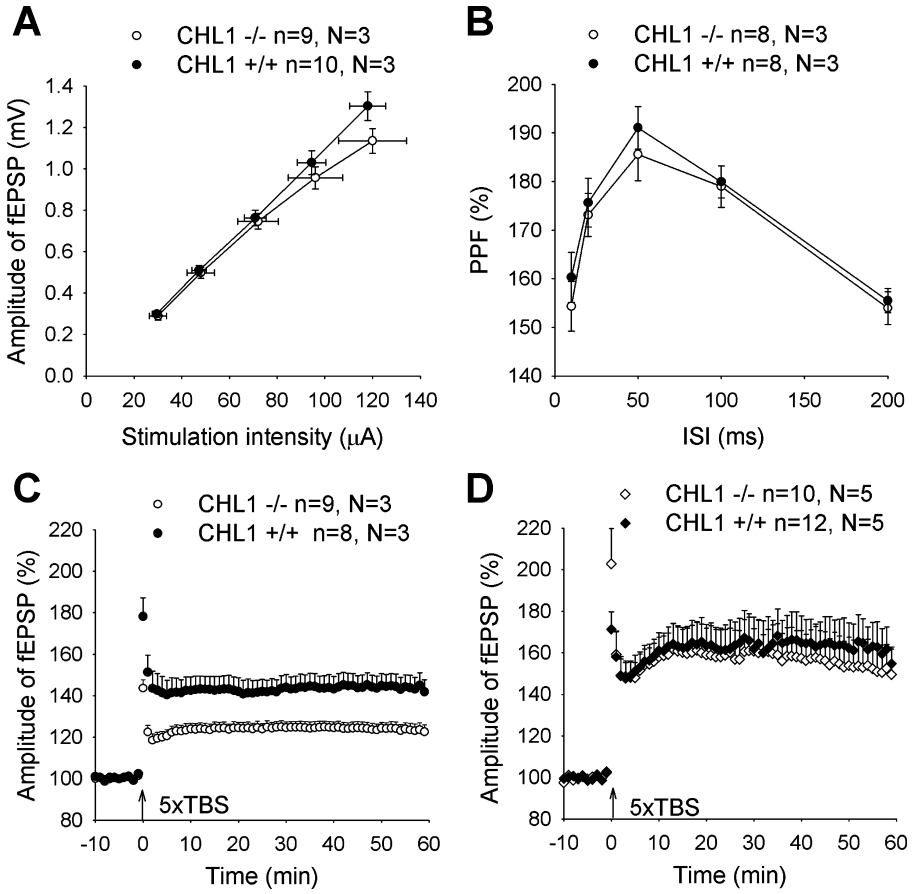

FIG. 4. Analysis of long-term potentiation. (A) Stimulus-response plots for fEPSPs evoked in the CA1 region by stimulation of CA3 pyramidal cell axons at different stimulation intensities. (B) Paired-pulse facilitation with 10, 20, 50, 100 and 200 ms inter-stimulus intervals. (C and D) Post-tetanic and long-term potentiation induced by five trains of theta-burst stimulation (TBS) in normal ACSF (C) and in the presence of 100 μM pictrotoxin (D). Mean amplitudes of fEPSPs recorded 0–10 min before induction of LTP were set to 100%. Numbers of analysed slices (*n*) and animals (*N*) are indicated.

different types of basket cell, PV^+ cholecystokinin-negative (CCK^-) and PV^- CCK^+ (Maccaferri *et al*., 2000; Somogyi & Klausberger, 2005). We addressed the question as to whether the PV^+ and PV^- GABAergic perisomatic inputs were similarly or differentially altered in the mutant mice. We quantified the number of perisomatic puncta positive for both PV and VGAT and such only positive for VGAT around the cell bodies of pyramidal neurons (Fig. 6A). VGAT was detected in puncta but not in fibres indicating that it is detectable in axon terminals and presumably confined to synapses. PV was detected in cell bodies, dendrites, axons and axon terminals. Therefore, we counted only perisomatic PV^+ puncta colabelled with VGAT, which are likely to be synapses. The results of the quantitative analysis revealed higher linear densities of both PV^+ and PV^- perisomatic puncta in CHL1–/– mice compared with wild-type littermates (+22% and +31%, respectively, Fig. 7A, B and D). The total density (PV^+ plus PV^- puncta) was increased by 27%. This result is in good agreement with the electron microscopic finding of increased coverage of cell bodies with active zones. The difference in the relative increase in CHL1–/– animals compared with CHL+/+ mice estimated by the two methods (+27% and +46%) is explainable by the assumption that large PV^+ $VGAT^+$ puncta contain, on average, more than one active zone. The results of the quantitative immunohistochemical analysis suggest that increased synaptic coverage in the mutant mice is due to increased input from both PV^+ and PV^- interneurons.

The digitized confocal images were also used to estimate the size of the pyramidal cell bodies. Soma areas were similar in CHL1–/– and CHL+/+ mice as indicated by comparisons of the frequency distributions and the group mean values (Fig. 7C and D). From this observation it can be concluded that the linear densities of active zones and perisomatic puncta are proportional to the numbers of active zones/puncta, i.e. synaptic input, per cell.

Analysis of parvalbumin-positive interneurons in CHL1–/– mice

The increased density of perisomatic inhibitory contacts in CHL1–/– mice could result from higher numbers of projecting interneurons. We performed a quantitative analysis of PV^+ cells in the CA1 field of the hippocampus (Fig. 8A). The numerical density (number of cells per unit volume) of these interneurons was almost twice as high in mutant compared with wild-type mice (Fig. 8B, 'Density'). As the estimated volume of the CA1 region in the dorsal hippocampus was similar in the two groups (Fig. 8B, 'Volume'), the total numbers were proportional to the densities (Fig. 8B, 'Number'). The total number of pyramidal neurons was also higher in the CHL1–/– animals compared with CHL1+/+ mice (Fig. 8C, 'Number') but this difference was much smaller (+13%) relative to the difference in the number of PV^+ interneurons (+94%). Thus, the ratio of PV^+ to pyramidal cells was significantly higher in the CHL1–/– animals (Fig. 8C, 'PV^+/pyramidal cells') indicating that a single pyramidal neuron is innervated by a higher-than-normal number of interneurons. In addition to PV^+ interneurons, it was of interest to analyse CCK positive neurons. This investigation could not be performed because antibodies of quality suitable for stereological analysis of CCK positive cells in mice were not available to us.

The impact of the CHL1 deficiency on the size of the PV^+ cell population raised the question as to whether cell morphology, in

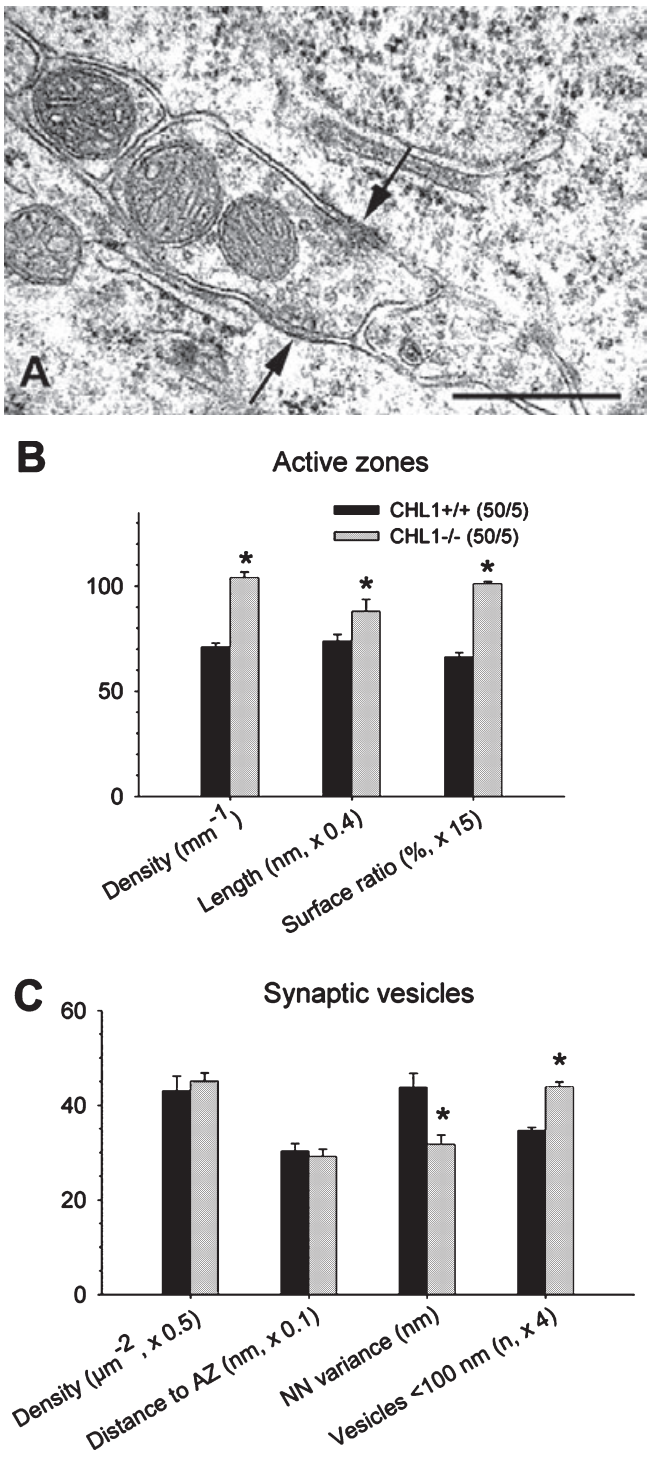

FIG. 5. Ultrastructural analysis of perisomatic synapses. (A) Electron micrograph of a perisomatic synapse with symmetric synaptic densities (arrows) in the CA1 pyramidal cell layer of a CHL1–/– mice. Scale bar, 500 nm. (B) Linear densities, length and surface ratio of active zones. Number of synapses/animals are indicated. (C) Density (number per unit area), distance to active zones, first nearest neighbour NN variance of synaptic vesicles and number of vesicles per terminal located closer than 100 nm from active zones. The number of vesicles studied was 2816 for CHL1+/+ mice and 3269 for CHL1–/– animals (50 synapses per genotype). (B and C) Shown are mean values + SEM. *$P < 0.05$, *t*-test, comparing the group mean values.

particular cell size, was influenced by the mutation. We measured the soma areas of randomly sampled PV^+ interneurons and found no difference between CHL1–/– and CHL1+/+ mice. The mean soma area in CHL1–/– mice was 213 ± 30 μm^2 (147 cells measured in four animals) and 214 ± 32 μm^2 (142 cells, four animals) in CHL1+/+ mice ($P > 0.05$, *t*-test). The frequency distribution histograms of the areas were bell-shaped in mice of both genotypes (data not shown) and distributions in CHL–/– and CHL1+/+ mice were not different ($P > 0.05$, Kolmogorov–Smirnov test).

Expression of CHL1 mRNA and protein

Previous morphological observations on CHL1 expression have been restricted to mRNA detection in brain sections of very young (1–3-week-old) mice. CHL1 mRNA expression has been observed in principal neurons and interneurons in the hypothalamus (Holm *et al.*, 1996) and stellate, basket, Golgi and granule cells in the cerebellar cortex (Hillenbrand *et al.*, 1999). In this study we confirmed these observations (data not shown) and found that, despite a decline in expression between 1 and 3 weeks, mRNA continues to be detectable until the age of one year (eight wild-type mice studied at ages of 1, 3 and 12 months, Fig. 9A and B). Using a commercial antibody raised against mouse CHL1, we could also detect and, for the first time, report on the expression pattern of CHL1 protein in the hippocampus (Fig. 6B; see also Supplementary material Fig. S1, E and F) and the cerebellar cortex (Supplementary material Fig. S1, A–D). CHL1 immunoreactivity was observed in all areas and layers of the hippocampus. Staining intensity was least prominent in the principal cell layers and highest in the hilus of the dentate gyrus and the mossy fibres in CA3 (Supplementary material Fig. S1, F and E, respectively). Enhanced, compared with the immediate surrounding, was labelling of interneuron cell bodies throughout the hippocampus. To reveal whether this expression was confined to a subpopulation of interneurons, for example PV^+ or PV^-, we used WFA to visualize perineuronal nets around PV^+ neurons. Previous work has shown that WFA-positive perineuronal nets surround predominantly, in 94–98% of all cases, PV^+ cells in the cerebral cortex of rodents (Wegner *et al.*, 2003; Irintchev *et al.*, 2005). Analysis of sections double-stained with WFA and PV antibody in the present study revealed that WFA is also a reliable marker for PV^+ cells in the hippocampus; 196 out of 221 cell profiles (89%) labelled with WFA were also PV-positive in the CA1 regions of wild-type mice (20 sections from five animals studied). WFA was used as a marker for PV^+ interneurons, and not PV itself, because in preliminary experiments we noticed interference between the PV and CHL1 staining upon double-labelling but not when WFA was combined with CHL1 antibody staining. Analysis of sections stained with WFA and CHL1 antibody showed that CHL1 was expressed in both WFA-positive and WFA-negative cells (Fig. 6B). The general conclusion from the results described above is that CHL1 is expressed in principal cells and interneurons of different chemical specificities in the hippocampus during early postnatal life and in adulthood.

Discussion

Our results provide first evidence that perisomatic inhibition is abnormally high in constitutively deficient juvenile CHL1 mice, as assessed by electrophysiological analysis of evoked unitary perisomatic IPSCs, electron microscopic evaluation of number and architecture of perisomatic symmetric synapses, and light microscopic analysis of interneurons in the CA1 region of the hippocampus.

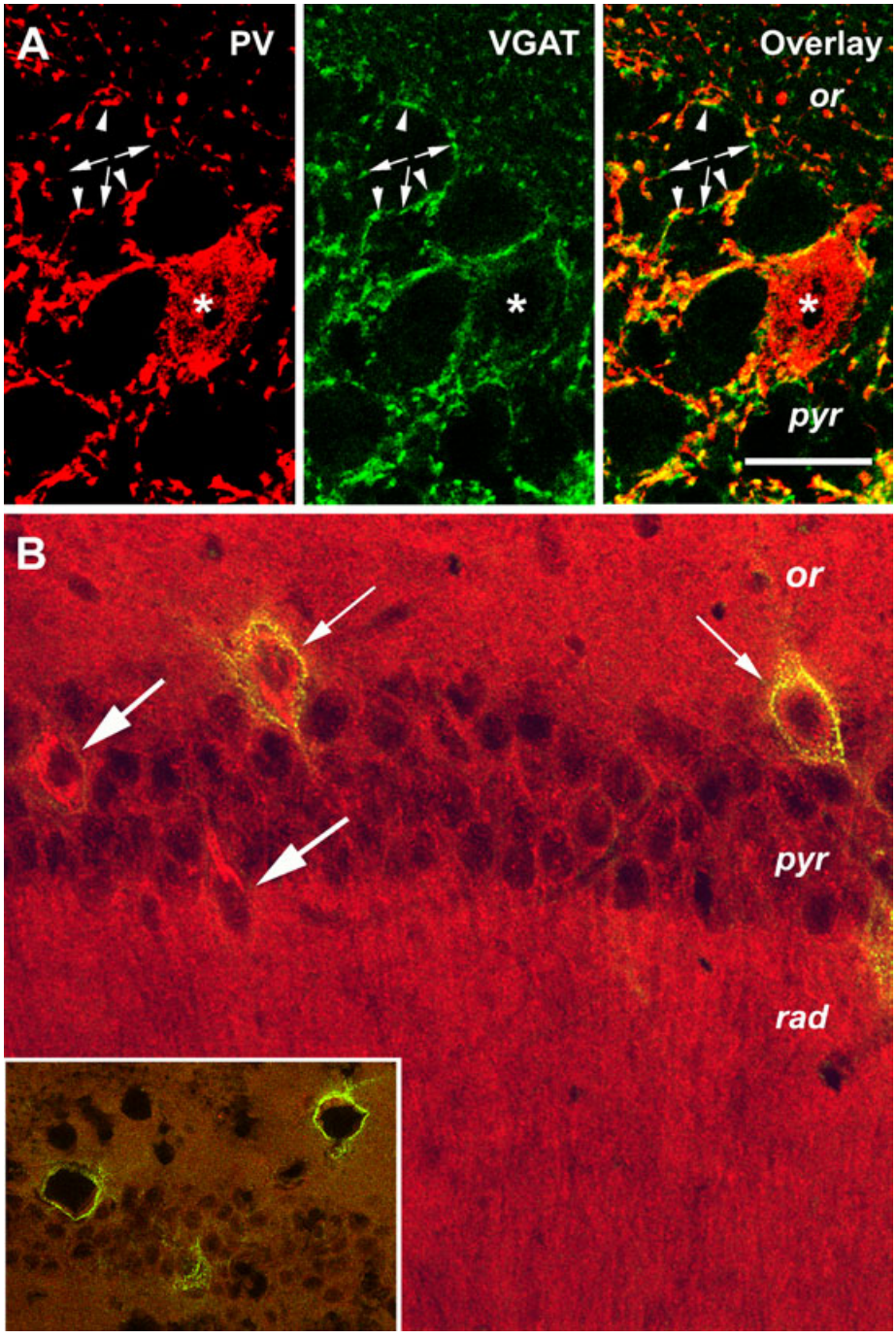

FIG. 6. Perisomatic puncta around pyramidal cells labelled with interneuron markers (A) and expression of CHL1 in interneurons (B) in the CA1 region. (A) Double immunostaining using antibodies against parvalbumin (PV, left panel) and vesicular GABA transporter (VGAT, middle panel) seen in a 1-μm-thick confocal slice (CHL1–/– mouse, 25-μm-thick coronal cryostat section). An overlay of immunostainings is shown in the right panel. For evaluation of perisomatic puncta, numbers of individually discernible PV^+ $VGAT^+$ (arrowheads) and PV^- $VGAT^+$ (arrows) were counted at the level of the largest cross-sectional area of individual cells determined by comparing the cell appearance in a stack of confocal slices. The asterisk marks a PV^+ interneuron. (B) Staining for CHL1 with a polyclonal antibody is widely seen in *strata orients* and *radiatum*, and in interneurons surrounded by perineuronal nets brightly labelled with WFA (thin arrows) in superimposed images from 5-μm-thick stacks of confocal slices from a 4-week-old CHL1+/+ mouse and a CHL1–/– littermate (25-μm-thick coronal brain sections). Compared with the overall diffuse antibody labelling, CHL1 staining in cells surrounded by perineuronal nets (thin arrows) and individual cells without nets (thick arrows), which are also interneurons as indicated by size and location, is more intense (A). Weak background CHL staining is seen in the section from the CHL1-deficient mouse (insert), whereas perineuronal nets are intensively labelled for WFA as in sections from wild-type mice. Labels indicate the layers of CA1, strata oriens (or), pyramidale (pyr) and radiatum (rad) in both panels. Scale bar, 20 μm (A); 60 μm (B) and 150 μm for the insert in (B). This figure is reproduced in colour on-line.

Abnormalities in synaptic transmission and their putative structural correlates

Electrophysiological analysis of inhibitory synaptic transmission revealed a 50% increase in the amplitude of minimal, presumably unitary, IPSCs in CHL1–/– mice compared with CHL1+/+ littermates. As coverage of pyramidal cell bodies by active zones was also found to be 50% higher in mutant mice, without change in soma size, one could assume that enhancement of evoked transmitter release is simply due to higher numbers of synapses. However, another line of evidence suggests a more plausible alternative explanation. Numbers of PV^+ interneurons in mutant mice were abnormally high and the ratio of PV^+ cells to pyramidal neurons was increased by more than 60%, indicating a smaller contribution of one interneuron to the synaptic coverage of an individual principal neuron. Therefore, we suggest that the increase in IPSC amplitudes in mutant mice is most likely related to increased synaptic efficacy rather than number of synapses. This conclusion will hold true if the detected increase in the size of the heterogeneous PV^+ cell population, including basket, axo-axonic, bistratified and oriens – lacunosum moleculare cells, reflects an increase in the perisomatically projecting cells among these cell types, i.e. the PV^+ basket cells (Maccaferri *et al*., 2000; Somogyi & Klausberger, 2005). We have no direct evidence for this. On the basis of the finding that CHL1 is expressed by different types of interneurons, perhaps by all interneurons in the hippocampus, we can assume that there is no differential influence of the mutation on subpopulations of PV^+ interneurons. This notion is supported by the

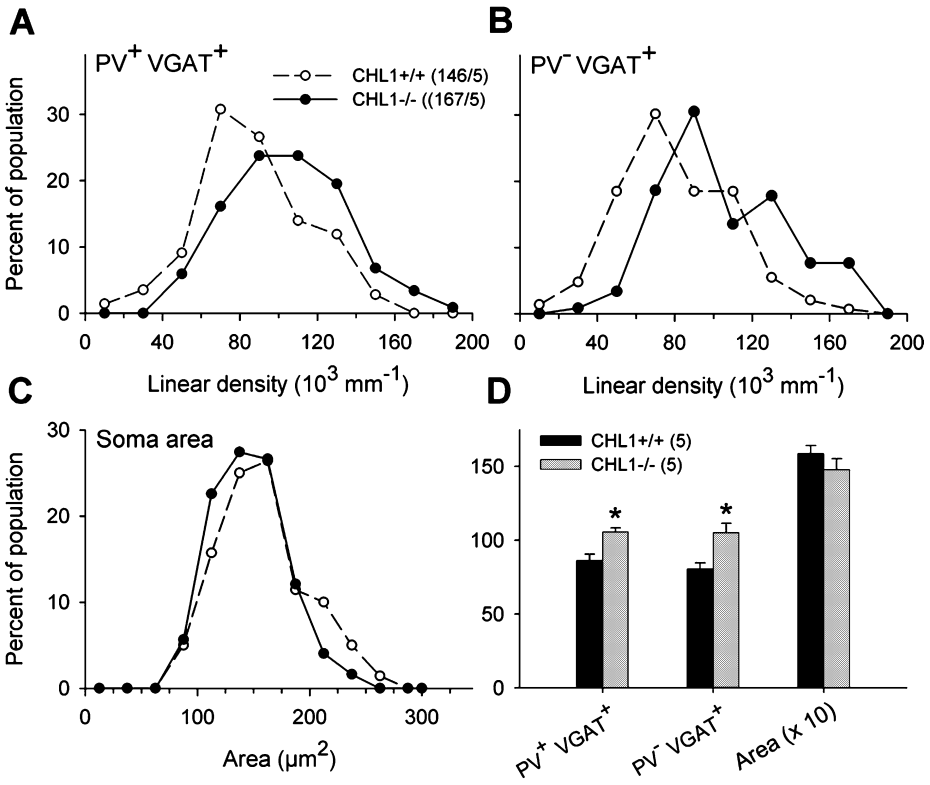

FIG. 7. Estimates of linear densities of perisomatic puncta around pyramidal cell bodies (A, B and D) and pyramidal cell size (C and D). Normalized frequency distribution histograms of linear densities of PV^+ $VGAT^+$ (A) and PV^- $VGAT^+$ (B) perisomatic puncta, and soma areas of pyramidal cells (C) in CHL1+/+ and CHL–/– mice. Number of cells/animals studied per genotype are indicated in the legend in (A). (D) Group mean values of the parameters shown in (A–C) calculated from individual mean values. *$P < 0.05$, *t*-test. Comparisons of the frequency distributions using Kolmogorov–Smirnov test revealed differences ($P < 0.05$) for linear densities of PV^+ $VGAT^+$ (A) and PV^- $VGAT^+$ (B) but not for soma areas (C, $P > 0.05$).

finding of increased numbers of PV^- $VGAT^+$ perisomatic puncta indicating increased input to the pyramidal cell bodies from interneurons other than the PV^+ basket cells, for example CCK^+ PV^- basket cells. Expression of CHL1 in PV^- interneurons suggests that such populations are affected by the mutation in a way similar to the PV^+ cells.

The increase in the mean amplitude of evoked IPSCs without detectable changes in the amplitude of the miniature IPSCs indicates that probability of release or number of vesicles available for release are increased in CHL1–/– mice. The electron microscopic analysis showed that the size of active zones in inhibitory synapses is increased. It is tempting to speculate that this feature represents a structural correlate of enhanced transmitter release in CHL1–/– mice. The size of an active zone is thought to be related to the functional efficacy of a synapse (Trommald & Hulleberg, 1997). It has been shown that in the CA1 field of the murine hippocampus the length of active zones of excitatory synapses correlates with the relative size of the docked pool of synaptic vesicles and, correspondingly, with vesicle release probability in excitatory synapses (Schikorski & Stevens, 1997). Our data show increased amplitudes of unitary pIPSCs and length of active zone profiles of perisomatic inhibitory synapses in CHL1–/– mice, suggesting that similar relationships may also hold true for inhibitory synapses. Interestingly, despite the increase in evoked release and number of inhibitory contacts, frequencies of miniature IPSCs were not elevated in CHL1–/– mice. Together with results showing that the number of inhibitory active zones per pyramidal cell is higher in mutants, we speculate that the rate of spontaneous asynchronous release per synaptic contact may be lower in CHL1–/– mice. These data highlights the possibility that abnormalities in GABA release in CHL1–/– mice could involve different mechanisms between spontaneous and evoked vesicle release. For instance, spontaneous GABA release has a lower sensitivity to Ca^{2+}/Mg^{2+}, and $GABA_B$ receptor agonist baclofen when compared with stimulus-evoked responses (Otis & Mody, 1992). There are other examples where changes in the two modes of release are dissociated (Taniguchi *et al.*, 2000; Saghatelyan *et al.*, 2001). Moreover, recent data indicate that spontaneously recycling vesicles and activity-dependent recycling vesicles originate from distinct pools (Sara *et al.*, 2005).

An additional factor related to the increased efficacy of GABAergic synapses in CHL1–/– mice may be related to closer location of synaptic vesicles to active zones of inhibitory synapses. It is well known that synaptic vesicles can be divided into several interconnected pools, with vesicles most proximal to active zones having the highest release-competence. Thus, the position of these organelles relative to active zones seems to be a reasonable morphological correlate of vesicle release-competence. In fact, the spatial arrangement of synaptic vesicles within the presynaptic terminal correlates with changes in the electrical activity of a synapse (Applegate & Landfield, 1988; Tyler & Pozzo-Miller, 2001). Although no significant difference was found in the number of synaptic vesicle profiles per presynaptic terminal profile between CHL1–/– and CHL1+/+ mice, our data indicate that the spatial arrangement of synaptic vesicles is different in the two genotypes. Higher numbers of synaptic vesicles were located very close to active zones (< 100 nm) in CHL1–/– mice and the overall intervesicle spacing variability was lower compared with CHL1+/+ mice. These structural features and the physiological abnormalities suggest that CHL1 is involved in regulation of the transmitter release machinery of inhibitory synapses.

Effects of constitutive CHL1 deficiency on inhibitory and excitatory neurons

Previous studies have shown that CHL1 deficiency causes aberrations in the mossy fibre and olfactory axon projections, and in positioning and shape of pyramidal cortical neurons (Montag-Sallaz *et al.*, 2002;

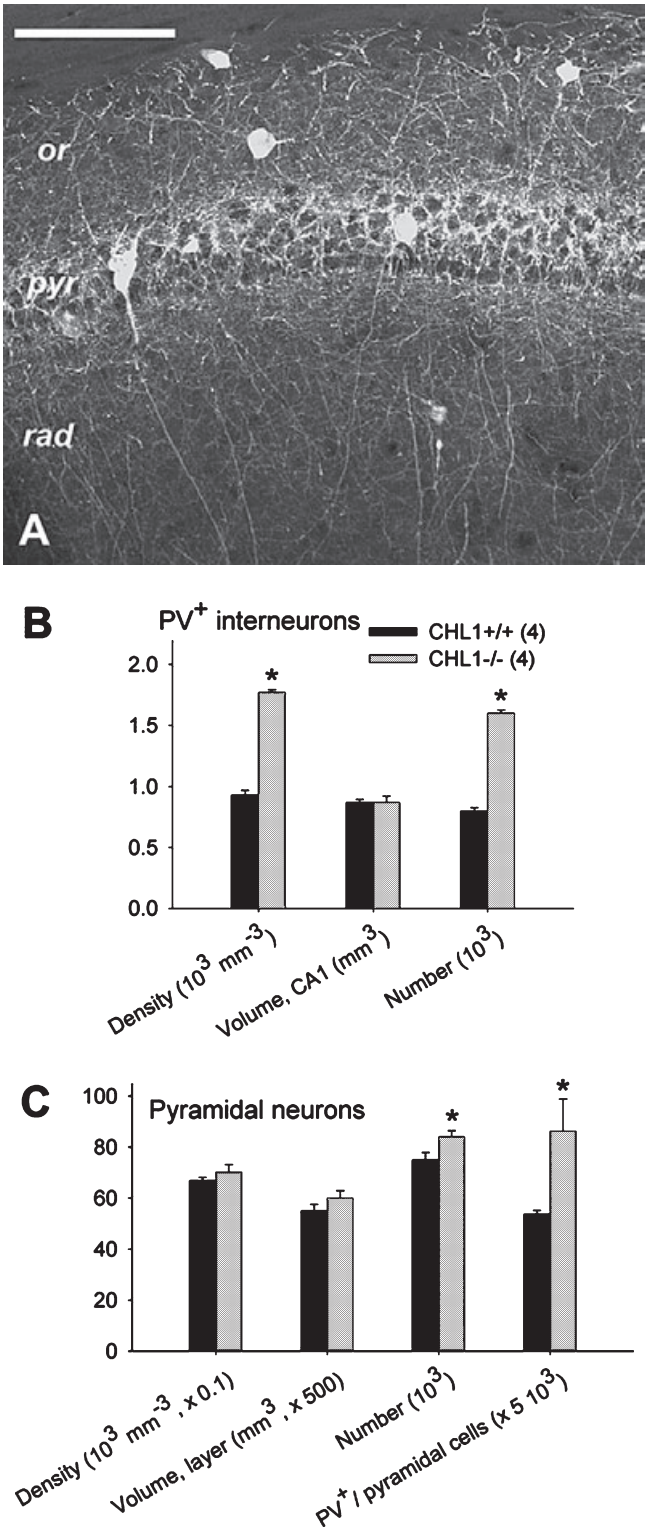

FIG. 8. Parvalbumin interneurons and principal cells in CA1. (A) Parvalbumin immunostaining in the CA1 region of a CHL1–/– mouse (25-μm-thick coronal cryostat section). Superimposed images from a 10-μm-thick stack of confocal slices. Labels indicate the layers of CA1, strata oriens (or), pyramidale (pyr) and radiatum (rad). Scale bar, 250 μm. (B and D) Mean values + SEM for numerical density ('Density'), volume of the CA1 region (B) and the pyramidal cell layer (C; 'Volume') and total number ('Number') of PV^+ cells (B) and pyramidal cells (C) in the dorsal hippocampus of CHL1+/+ and CHL1–/– mice. In C, the ratio of parvalbumin-positive to pyramidal cells is shown in addition. *$P < 0.05$, *t*-test.

Demyanenko *et al*., 2004). These findings, in conjunction with *in vitro* data (Hillenbrand *et al*., 1999), indicate that CHL1 is essential for axonal growth, path finding, synapse formation, neuronal migration and dendritic growth in certain brain regions. In this investigation, we found that deficient CHL1 expression also affects the size of two neuronal populations in the hippocampus: the numbers of both pyramidal cells and parvalbumin-immunoreactive interneurons are higher in mutant vs. wild-type mice. We also show, for the first time, that CHL1 is expressed in these neuronal cell types during early postnatal life and in adulthood. These findings support the idea of direct influences of CHL1 on the formation and maintenance of this neuronal population in the hippocampus. How CHL1 is implicated in proliferation of neuronal precursor cells, cell migration and/or cell death remains to be elucidated in future experiments. It is worth mentioning in this respect that CHL1 is a survival factor for cultured cerebellar and hippocampal neurons (Chen *et al*., 1999) and motoneurons (Nishimune *et al*., 2005) and stimulates cell migration (Buhusi *et al*., 2003). Therefore, it is unlikely that a deficit in CHL1 would promote survival or migration of neurons, putting forward the idea that expression of CHL1 may restrain proliferation of neuronal precursor cells, similarly to L1 (Dihne *et al*., 2003). Thus, the most plausible explanation for the observed increase in the number of both interneurons and principal neurons in the CA1 region is that during development more of these neurons are produced in CHL1–/– mice than in wild-type animals.

Functional implication of increased perisomatic inhibition in CHL1–/– mice

Parvalbumin-immunoreactive interneurons comprise a major proportion of the GABAergic cell population in the hippocampus. These inhibitory neurons, being coupled both chemically and electrically, form an inhibitory network that operates at high-frequency discharge rates (Fukuda & Kosaka, 2000; Galarreta & Hestrin, 2002; Freund, 2003). This network, establishing synapses on principal cells, has a strong impact on neuronal excitability and, thus, regulates basic physiological properties such as synchronization and oscillatory activities in the hippocampus. Therefore, it could be expected that an increased inhibitory synaptic input to pyramidal cells, combined with enhanced transmitter release at the level of individual synapses, would have profound effects on hippocampal functions. In fact, the dysbalance between excitation and inhibition may be related to the abnormal prepulse inhibition observed in CHL1 mutant mice (Irintchev *et al*., 2004). Previous studies have shown that prepulse inhibition is indeed impaired if excitation is reduced or inhibition is enhanced by pharmacological application of glutamate antagonists and GABA agonists, respectively (Geyer *et al*., 2001, 2002; Swerdlow *et al*., 2001).

GABAergic transmission is also important in regulation of synaptic plasticity. For instance, LTP is impaired in the dentate gyrus of anaesthetized and freely moving mice deficient in the cell adhesion molecule, Thy-1. The deficit in LTP in this mutant can be rescued by a $GABA_A$ receptor antagonist (Nosten-Bertrand *et al*., 1996; Errington *et al*., 1997) and there is an increase in inhibitory postsynaptic currents in the dentate gyrus of Thy-1 deficient mice (Hollrigel *et al*., 1998). Similarly, a deficit in CA1 LTP in mice overexpressing heparin-binding growth-associated molecule, HB-GAM, can be normalized by disinhibition of hippocampal slices and is accompanied by an increase in inhibitory currents (Pavlov *et al*., 2006). Our data on impaired LTP in CHL1–/– mice provide another example of regulation of LTP via an increase in levels of GABAergic inhibition.

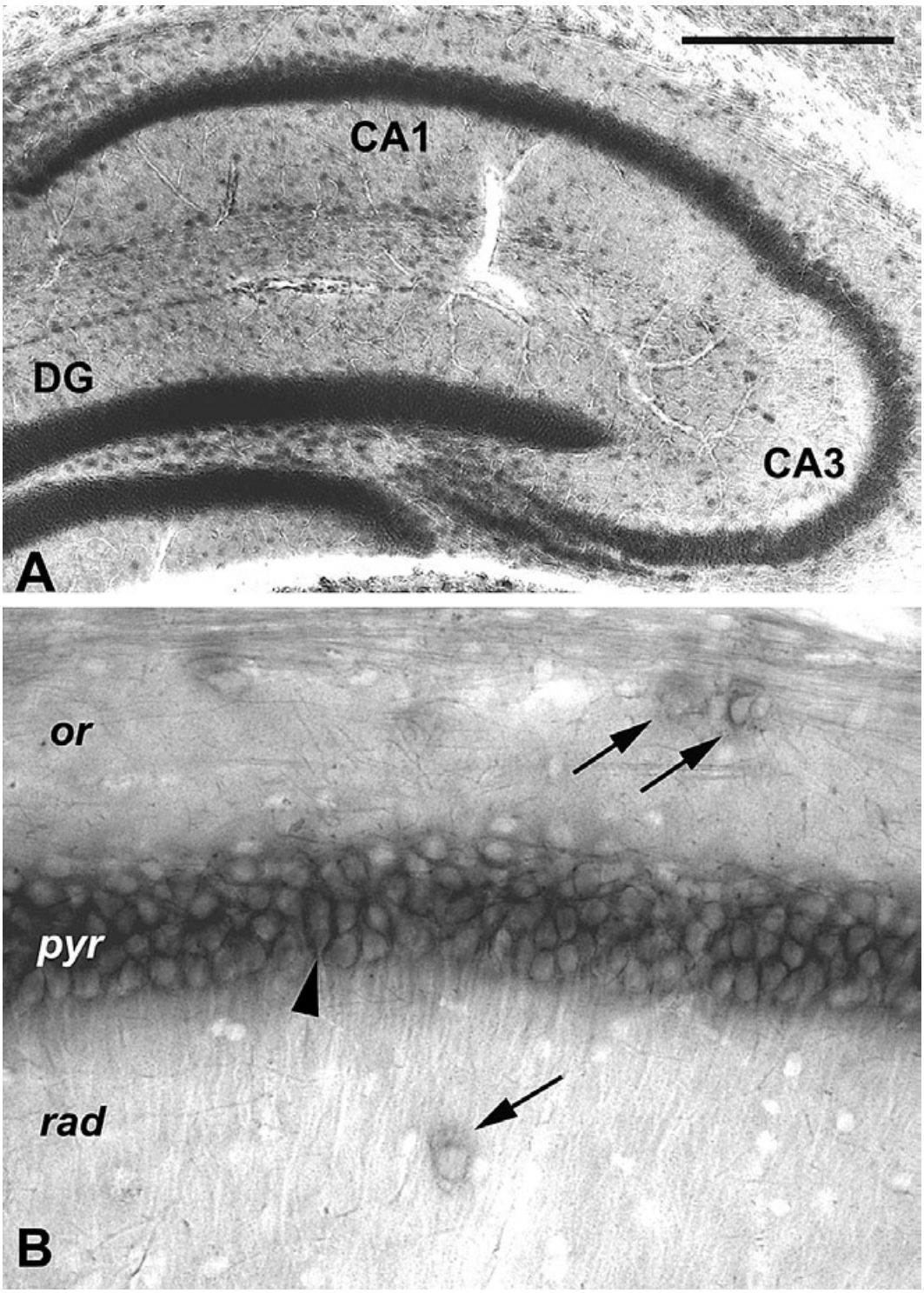

FIG. 9. Detection of CHL1 mRNA. *In situ* hybridization using an antisense CHL1 probe and 70-μm-thick free-floating coronal brain sections from a 4-week-old (A, low-power magnification of the whole hippocampal formation) and a 3-month-old (B, high-magnification view of the CA1 region) wild-type mouse. Labels in A indicate the CA1 and CA3 region and the dentate gyrus (DG). Arrows in B point to individual positive interneurons in the oriens (or) and radiatum (rad) layers of CA1. Note a large-diameter positive cell profile (arrowhead) in the pyramidal (pyr) layer. Scale bar, 1 mm (A) and 250 μm (B).

In contrast to these mutants, mice deficient in L1 or the extracellular glycoprotein tenascin-R have reduced perisomatic inhibition. Although the number of parvalbumin-immunoreactive interneurons are not significantly changed in L1-deficient and tenascin-R-deficient mice, the amplitudes of unitary perisomatic IPSCs are reduced (Saghatelyan *et al*., 2001, 2004) and this abnormality is accompanied by a reduction in the density and size of perisomatic inhibitory active zones and by alterations in the distribution of synaptic vesicles in inhibitory synapses (Nikonenko *et al*., 2003; Saghatelyan *et al*., 2004). Finally, a number of *in vitro* studies indicate that neuroligins and their

synaptic binding partners modulate the development of both excitatory and inhibitory synapses (for a recent review, see Levinson & El Husseini, 2005). Thus, several extracellular matrix and cell adhesion molecules, including CHL1 appear to be crucial for generation and maintenance of GABAergic cells and synapses. However, the specific role of CHL1 – at least on the basis of the available data – lies in up-regulation of both the number of interneurons and the efficacy of GABAergic synapses.

Acknowledgements

We are grateful to Drs Udo Bartsch and Igor Jakovcevski for advice on *in situ* hybridization, Emanuela Szpotowicz for technical assistance, Eva Kronenberg for animal care and Achim Dahlmann for genotyping. This work was supported by the Deutsche Forschungsgemeinschaft (SCHA 185/38 to M.S. and Di702/5 to A.D.) and Deutscher Akademischer Austauschdienst (to M.S.).

Supplementary material

The following supplementary material may be found on http://www.blackwell-synergy.com

Fig. S1. Immunohistochemical detection of CHL1 in the cerebellum, the CA3 region of the hippocampus and the dentate gyrus.

Abbreviations

ACSF, artificial cerebrospinal fluid; CHL1, close homologue of L1; fEPSP, field excitatory postsynaptic potentials; IPSC, inhibitory postsynaptic currents; LTP, long-term potentiation; mIPSC, miniature inhibitory postsynaptic currents; pIPSCs, perisomatic inhibitory postsynaptic currents; PV, parvalbumin; PV^+, parvalbumin-positive; VGAT, vesicular GABA transporter; SEM, standard error of the mean; WFA, *Wisteria floribunda* agglutinin.

References

Applegate, M.D. & Landfield, P.W. (1988) Synaptic vesicle redistribution during hippocampal frequency potentiation and depression in young and aged rats. *J. Neurosci.*, **8**, 1096–1111.

Banks, M.I., Li, T.B. & Pearce, R.A. (1998) The synaptic basis of GABAA, slow. *J. Neurosci.*, **18**, 1305–1317.

Bartsch, S., Bartsch, U., Dorries, U., Faissner, A., Weller, A., Ekblom, P. & Schachner, M. (1992) Expression of tenascin in the developing and adult cerebellar cortex. *J. Neurosci.*, **12**, 736–749.

Buhusi, M., Midkiff, B.R., Gates, A.M., Richter, M., Schachner, M. & Maness, P.F. (2003) Close homolog of L1 is an enhancer of integrin-mediated cell migration. *J. Biol. Chem.*, **278**, 25024–25031.

Chaisuksunt, V., Zhang, Y., Anderson, P.N., Campbell, G., Vaudano, E., Schachner, M. & Lieberman, A.R. (2000a) Axonal regeneration from CNS neurons in the cerebellum and brainstem of adult rats: correlation with the patterns of expression and distribution of messenger RNAs for L1, CHL1, c-jun and growth-associated protein-43. *Neuroscience*, **100**, 87–108.

Chaisuksunt, V., Campbell, G., Zhang, Y., Schachner, M., Lieberman, A.R. & Anderson, P.N. (2000b) The cell recognition molecule CHL1 is strongly upregulated by injured and regenerating thalamic neurons. *J. Comp. Neurol.*, **425**, 382–392.

Chen, S., Mantei, N., Dong, L. & Schachner, M. (1999) Prevention of neuronal cell death by neural adhesion molecules L1 and CHL1. *J. Neurobiol.*, **38**, 428–439.

Chen, Q.Y., Chen, Q., Feng, G.Y., Lindpaintner, K., Chen, Y., Sun, X., Chen, Z., Gao, Z., Tang, J. & He, L. (2005) Case–control association study of the close homologue of L1 (CHL1) gene and schizophrenia in the Chinese population. *Schizophr. Res.*, **73**, 269–274.

Demyanenko, G.P., Schachner, M., Anton, E., Schmid, R., Feng, G., Sanes, J. & Maness, P.F. (2004) Close homolog of L1 modulates area-specific neuronal positioning and dendrite orientation in the cerebral cortex. *Neuron*, **44**, 423–437.

Demyanenko, G.P., Tsai, A.Y. & Maness, P.F. (1999) Abnormalities in neuronal process extension, hippocampal development, and the ventricular system of L1 knockout mice. *J. Neurosci.*, **19**, 4907–4920.

Dihne, M., Bernreuther, C., Sibbe, M., Paulus, W. & Schachner, M. (2003) A new role for the cell adhesion molecule L1 in neural precursor cell proliferation, differentiation, and transmitter-specific subtype generation. *J. Neurosci.*, **23**, 6638–6650.

Dörries, U., Bartsch, U., Nolte, C., Roth, J. & Schachner, M. (1993) Adaptation of a non-radioactive *in situ* hybridization method to electron microscopy: detection of tenascin mRNAs in mouse cerebellum with digoxigenin-labelled probes and gold-labelled antibodies. *Histochemistry*, **99**, 251–262.

Errington, M.L., Bliss, T.V., Morris, R.J., Laroche, S. & Davis, S. (1997) Long-term potentiation in awake mutant mice. *Nature*, **387**, 666–667.

Franklin, K.B.J. & Paxinos, G. (1997) *The Mouse Brain in Stereotaxic Coordinates*. Academic Press, San Diego.

Freund, T.F. (2003) Interneuron Diversity series: Rhythm and mood in perisomatic inhibition. *TINS*, **26**, 489–495.

Frints, S.G., Marynen, P., Hartmann, D., Fryns, J.P., Steyaert, J., Schachner, M., Rolf, B., Craessaerts, K., Snellinx, A., Hollanders, K., D'Hooge, R., De Deyn, P.P. & Froyen, G. (2003) CALL interrupted in a patient with non-specific mental retardation: gene dosage-dependent alteration of murine brain development and behavior. *Hum. Mol. Genet.*, **12**, 1463–1474.

Fukuda, T. & Kosaka, T. (2000) The dual network of GABAergic interneurons linked by both chemical and electrical synapses: a possible infrastructure of the cerebral cortex. *Neurosci. Res.*, **38**, 123–130.

Galarreta, M. & Hestrin, S. (2002) Electrical and chemical synapses among parvalbumin fast-spiking GABAergic interneurons in adult mouse neocortex. *Proc. Natl Acad. Sci. USA*, **99**, 12438–12443.

Geyer, M.A., Krebs-Thomson, K., Braff, D.L. & Swerdlow, N.R. (2001) Pharmacological studies of prepulse inhibition models of sensorimotor gating deficits in schizophrenia: a decade in press. *Psychopharmacology (Berl)*, **156**, 117–154.

Geyer, M.A., McIlwain, K.L. & Paylor, R. (2002) Mouse genetic models for prepulse inhibition: an early review. *Mol. Psychiatry*, **7**, 1039–1053.

Gundersen, H.J. (1986) Stereology of arbitrary particles. A review of unbiased number and size estimators and the presentation of some new ones, in memory of William R. Thompson. *J. Microsc.*, **143**, 3–45.

Hillenbrand, R., Molthagen, M., Montag, D. & Schachner, M. (1999) The close homologue of the neural adhesion molecule L1 (CHL1): patterns of expression and promotion of neurite outgrowth by heterophilic interactions. *Eur. J. Neurosci.*, **11**, 813–826.

Hollrigel, G.S., Morris, R.J. & Soltesz, I. (1998) Enhanced bursts of IPSCs in dentate granule cells in mice with regionally inhibited long-term potentiation. *Proc. Biol. Sci.*, **265**, 63–69.

Holm, J., Hillenbrand, R., Steuber, V., Bartsch, U., Moos, M., Lubbert, H., Montag, D. & Schachner, M. (1996) Structural features of a close homologue of L1 (CHL1) in the mouse: a new member of the L1 family of neural recognition molecules. *Eur. J. Neurosci.*, **8**, 1613–1629.

Howard, C.V. & Reed, M.G. (1998) *Unbiased Stereology*. BIOS. Scientific Publishers, Oxford.

Irintchev, A., Koch, M., Needham, L.K., Maness, P. & Schachner, M. (2004) Impairment of sensorimotor gating in mice deficient in the cell adhesion molecule L1 or its close homologue, CHL1. *Brain Res.*, **1029**, 131–134.

Irintchev, A., Rollenhagen, A., Troncoso, E., Kiss, J.Z. & Schachner, M. (2005) Structural and functional aberrations in the cerebral cortex of tenascin-C deficient mice. *Cereb. Cortex*, **15**, 950–962.

Jiao, Y., Sun, Z., Lee, T., Fusco, F.R., Kimble, T.D., Meade, C.A., Cuthbertson, S. & Reiner, A. (1999) A simple and sensitive antigen retrieval method for free-floating and slide-mounted tissue sections. *J. Neurosci. Meth.*, **93**, 149–162.

Kenwrick, S., Watkins, A. & De Angelis, E. (2000) Neural cell recognition molecule L1: relating biological complexity to human disease mutations. *Hum. Mol. Genet.*, **9**, 879–886.

Kurumaji, A., Nomoto, H., Okano, T. & Toru, M, (2001) An association study between polymorphism of L1CAM gene and schizophrenia in a Japanese sample. *Am. J. Med. Genet.*, **105**, 99–104.

Levinson, J.N. & El Husseini, A. (2005) Building excitatory and inhibitory synapses: balancing neuroligin partnerships. *Neuron*, **48**, 171–174.

Lewis, D.A., Hashimoto, T. & Volk, D.W. (2005) Cortical inhibitory neurons and schizophrenia. *Nature Rev. Neurosci.*, **6**, 312–324.

Lewis, C.M., Levinson, D.F., Wise, L.H., DeLisi, L.E., Straub, R.E., Hovatta, I., Williams, N.M., Schwab, S.G., Pulver, A.E., Faraone, S.V., Brzustowicz, L.M., Kaufmann, C.A., Garver, D.L., Gurling, H.M., Lindholm, E., Coon, H., Moises, H.W., Byerley, W., Shaw, S.H., Mesen, A., Sherrington, R., O'Neill, F.A., Walsh, D., Kendler, K.S., Ekelund, J., Paunio, T., Lonnqvist, J., Peltonen, L., O'Donovan, M.C., Owen, M.J., Wildenauer, D.B., Maier, W., Nestadt, G., Blouin, J.L., Antonarakis, S.E., Mowry, B.J., Silverman, J.M., Crowe, R.R., Cloninger, C.R., Tsuang, M.T., Malaspina, D., Harkavy-Friedman, J.M., Svrakic, D.M., Bassett, A.S., Holcomb, J., Kalsi, G.,

McQuillin, A., Brynjolfson, J., Sigmundsson, T., Petursson, H., Jazin, E., Zoega, T. & Helgason, T. (2003) Genome scan meta-analysis of schizophrenia and bipolar disorder, part II: Schizophrenia. *Am. J. Hum. Genet.*, **73**, 34–48.

Long, J.M., Kalehua, A.N., Muth, N.J., Hengemihle, J.M., Jucker, M., Calhoun, M.E., Ingram, D.K. & Mouton, P.R. (1998) Stereological estimation of total microglia number in mouse hippocampus. *J. Neurosci. Meth.*, **84**, 101–108.

Maccaferri, G., Roberts, J.D., Szucs, P., Cottingham, C.A. & Somogyi, P. (2000) Cell surface domain specific postsynaptic currents evoked by identified GABAergic neurones in rat hippocampus *in vitro*. *J. Physiol.*, **524**, 91–116.

Montag-Sallaz, M., Schachner, M. & Montag, D. (2002) Misguided axonal projections, neural cell adhesion molecule 180 mRNA upregulation, and altered behavior in mice deficient for the close homolog of L1. *Mol. Cell. Biol.*, **22**, 7967–7981.

Nikonenko, A., Schmidt, S., Skibo, G., Bruckner, G. & Schachner, M. (2003) Tenascin-R-deficient mice show structural alterations of symmetric perisomatic synapses in the CA1 region of the hippocampus. *J. Comp. Neurol.*, **456**, 338–349.

Nishimune, H., Bernreuther, C., Carroll, P., Chen, S., Schachner, M. & Henderson, C.E. (2005) Neural adhesion molecules L1 and CHL1 are survival factors for motoneurons. *J. Neurosci. Res.*, **80**, 593–599.

Nosten-Bertrand, M., Errington, M.L., Murphy, K.P., Tokugawa, Y., Barboni, E., Kozlova, E., Michalovich, D., Morris, R.G., Silver, J., Stewart, C.L., Bliss, T.V. & Morris, R.J. (1996) Normal spatial learning despite regional inhibition of LTP in mice lacking Thy-1. *Nature*, **379**, 826–829.

Otis, T.S. & Mody, I. (1992) Modulation of decay kinetics and frequency of GABAA receptor-mediated spontaneous inhibitory postsynaptic currents in hippocampal neurons. *Neuroscience*, **49**, 13–32.

Pavlov, I., Rauvala, H. & Taira, T. (2006) Enhanced hippocampal gabaergic inhibition in mice overexpressing heparin-binding growth-associated molecule. *Neuroscience.* In press.

Peters, A., Palay, S. & Webster, H. (1991) *The Fine Structure of the Nervous System: Neurons and Their Supporting Cells*. Oxford University Press, Oxford.

Rolf, B., Lang, D., Hillenbrand, R., Richter, M., Schachner, M. & Bartsch, U. (2003) Altered expression of CHL1 by glial cells in response to optic nerve injury and intravitreal application of fibroblast growth factor-2. *J. Neurosci. Res.*, **71**, 835–843.

Saghatelyan, A.K., Dityatev, A., Schmidt, S., Schuster, T., Bartsch, U. & Schachner, M. (2001) Reduced perisomatic inhibition, increased excitatory transmission, and impaired long-term potentiation in mice deficient for the extracellular matrix glycoprotein tenascin-R. *Mol. Cell. Neurosci.*, **17**, 226–240.

Saghatelyan, A.K., Gorissen, S., Albert, M., Hertlein, B., Schachner, M. & Dityatev, A. (2000) The extracellular matrix molecule tenascin-R and its HNK-1 carbohydrate modulate perisomatic inhibition and long-term potentiation in the CA1 region of the hippocampus. *Eur. J. Neurosci.*, **12**, 3331–3342.

Saghatelyan, A.K., Nikonenko, A.G., Sun, M., Rolf, B., Putthoff, P., Kutsche, M., Bartsch, U., Dityatev, A. & Schachner, M. (2004) Reduced GABAergic transmission and number of hippocampal perisomatic inhibitory synapses in juvenile mice deficient in the neural cell adhesion molecule L1. *Mol. Cell. Neurosci.*, **26**, 191–203.

Sakurai, K., Migita, O., Toru, M. & Arinami, T. (2002) An association between a missense polymorphism in the close homologue of L1 (CHL1, CALL) gene and schizophrenia. *Mol. Psychiatry*, **7**, 412–415.

Sara, Y., Virmani, T., Deak, F., Liu, X. & Kavalali, E.T. (2005) An isolated pool of vesicles recycles at rest and drives spontaneous neurotransmission. *Neuron*, **45**, 563–573.

Schikorski, T. & Stevens, C.F. (1997) Quantitative ultrastructural analysis of hippocampal excitatory synapses. *J. Neurosci.*, **17**, 5858–5867.

Somogyi, P. & Klausberger, T. (2005) Defined types of cortical interneurone structure space and spike timing in the hippocampus. *J. Physiol.*, **562**, 9–26.

Stevens, C.F. & Wang, Y. (1994) Changes in reliability of synaptic function as a mechanism for plasticity. *Nature*, **371**, 704–707.

Swerdlow, N.R., Geyer, M.A. & Braff, D.L. (2001) Neural circuit regulation of prepulse inhibition of startle in the rat: current knowledge and future challenges. *Psychopharmacology (Berl)*, **156**, 194–215.

Taniguchi, N., Takada, N., Kimura, F. & Tsumoto, T. (2000) Actions of brain-derived neurotrophic factor on evoked and spontaneous EPSCs dissociate with maturation of neurones cultured from rat visual cortex. *J. Physiol.*, **527**, 579–592.

Torrey, E.F., Barci, B.M., Webster, M.J., Bartko, J.J., Meador-Woodruff, J.H. & Knable, M.B. (2005) Neurochemical markers for schizophrenia, bipolar disorder, and major depression in postmortem brains. *Biol. Psychiatry*, **57**, 252–260.

Trommald, M. & Hulleberg, G. (1997) Dimensions and density of dendritic spines from rat dentate granule cells based on reconstructions from serial electron micrographs. *J. Comp. Neurol.*, **377**, 15–28.

Tyler, W.J. & Pozzo-Miller, L.D. (2001) BDNF enhances quantal neurotransmitter release and increases the number of docked vesicles at the active zones of hippocampal excitatory synapses. *J. Neurosci.*, **21**, 4249–4258.

Van den Buuse, M., Garner, B. & Koch, M. (2003) Neurodevelopmental animal models of schizophrenia: effects on prepulse inhibition. *Curr. Mol. Med.*, **3**, 459–471.

Wegner, F., Hartig, W., Bringmann, A., Grosche, J., Wohlfarth, K., Zuschratter, W. & Bruckner, G. (2003) Diffuse perineuronal nets and modified pyramidal cells immunoreactive for glutamate and the GABA(A) receptor alpha1 subunit form a unique entity in rat cerebral cortex. *Exp. Neurol.*, **184**, 705–714.

Zhang, Y., Roslan, R., Lang, D., Schachner, M., Lieberman, A.R. & Anderson, P.N. (2000) Expression of CHL1 and L1 by neurons and glia following sciatic nerve and dorsal root injury. *Mol. Cell. Neurosci.*, **16**, 71–86.